AD-A165 953 ONE DIMENSIONAL MODELS FOR RELATIVISTIC ELECTRON BEAM DIODE DESIGN(U) NAVAL RESEARCH LAB WASHINGTON DC J M FINN ET AL. 28 FEB 86 NRL-MR-5727 1/1

UNCLASSIFIED F/G 9/1 NL

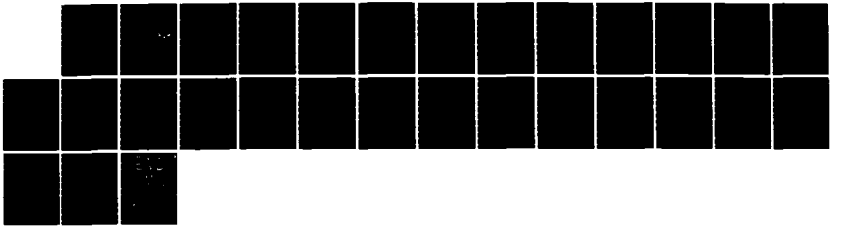

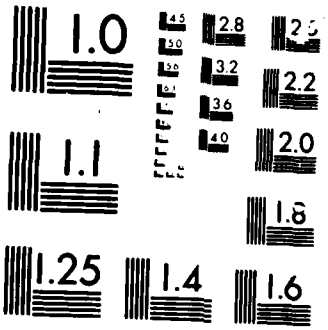

MICROCOPY RESOLUTION TEST CHART

NRL Memorandum Report 5727

One Dimensional Models for Relativistic Electron Beam Diode Design

JOHN M. FINN,* ARNE W. FLIFLET, AND WALLACE M. MANHEIMER

High Power Electromagnetic Radiation Branch
Plasma Physics Division

**Science Applications Inc.,*
McLean, VA 22102.

February 28, 1986

This work was sponsored in part by the Department of Energy in a cooperative program with the Lawrence Livermore National Laboratory.

NAVAL RESEARCH LABORATORY
Washington, D.C.

AD-A165953

SECURITY CLASSIFICATION OF THIS PAGE

REPORT DOCUMENTATION PAGE

1a. REPORT SECURITY CLASSIFICATION UNCLASSIFIED	1b. RESTRICTIVE MARKINGS
2a. SECURITY CLASSIFICATION AUTHORITY	3. DISTRIBUTION / AVAILABILITY OF REPORT Approved for public release; Distribution unlimited.
2b. DECLASSIFICATION / DOWNGRADING SCHEDULE	
4. PERFORMING ORGANIZATION REPORT NUMBER(S) NRL Memorandum Report 5727	5. MONITORING ORGANIZATION REPORT NUMBER(S)
6a. NAME OF PERFORMING ORGANIZATION Naval Research Laboratory 6b. OFFICE SYMBOL (If applicable)	7a. NAME OF MONITORING ORGANIZATION
6c. ADDRESS (City, State, and ZIP Code) Washington, D.C. 20375-5000	7b. ADDRESS (City, State, and ZIP Code)
8a. NAME OF FUNDING / SPONSORING ORGANIZATION (See page ii) 8b. OFFICE SYMBOL (If applicable)	9. PROCUREMENT INSTRUMENT IDENTIFICATION NUMBER
8c. ADDRESS (City, State, and ZIP Code) Arlington, VA 22217 Washington, D.C. 20305	10. SOURCE OF FUNDING NUMBERS PROGRAM ELEMENT NO: (See page ii) PROJECT NO: (See page ii) TASK NO.: (See page ii) WORK UNIT ACCESSION NO.: (See page ii)

11. TITLE (Include Security Classification)
One Dimensional Models for Relativistic Electron Beam Diode Design

12. PERSONAL AUTHOR(S)
John M. Finn, Arne W. Fliflet, and Wallace M. Manheimer

13a. TYPE OF REPORT	13b. TIME COVERED	14. DATE OF REPORT (Year, Month, Day)	15. PAGE COUNT
Interim	FROM 1/1/84 TO 4/30/85	1986 February 28	30

16. SUPPLEMENTARY NOTATION
*This work was sponsored in part by the Department of Energy in a cooperative program with the Lawrence Livermore National Laboratory.

17. COSATI CODES		
FIELD	GROUP	SUB-GROUP

18. SUBJECT TERMS (Continue on reverse if necessary and identify by block number)
Diodes, Velocity, Electron Beams, Microwave, Helical, Transverse Momentum, Spacial, Gyrotrons, Trajectory

19. ABSTRACT (Continue on reverse if necessary and identify by block number)

Several one dimensional models are derived which approximate the relativistic flow of high current beams in diodes. Using these models as a starting point, a diode for a 1 GW beam for a 35 GHz gyrotron oscillator is easily designed.

20. DISTRIBUTION / AVAILABILITY OF ABSTRACT ☐ UNCLASSIFIED/UNLIMITED X SAME AS RPT ☐ DTIC USERS	21. ABSTRACT SECURITY CLASSIFICATION UNCLASSIFIED
22a. NAME OF RESPONSIBLE INDIVIDUAL Arne W. Fliflet	22b. TELEPHONE (Include Area Code) 202/767-2469 22c. OFFICE SYMBOL Code 4740

DD FORM 1473, 84 MAR 83 APR edition may be used until exhausted
All other editions are obsolete

SECURITY CLASSIFICATION OF THIS PAGE

8a. NAME OF FUNDING/SPONSORING ORGANIZATION

Office of Naval Research
Defense Nuclear Agency and
Department of Energy*

10. SOURCE OF FUNDING NUMBERS

PROGRAM ELEMENT NO.	PROJECT NO.	TASK NO.	WORK UNIT ACCESSION NO.
61153N	47-0866-00	RR011-0941	DN880-06
62715H	47-2156-00	X99ZmXVF 84-607	DN480-686
	47-2138-00		DE-A103-84/SF12188

SYNOPSIS

The design of electron guns or diodes for high power microwave tubes is a complicated two dimensional spatial and three dimensional velocity space problem. It involves the calculation of non-linear particle orbits and self consistent electric and magnetic fields. The design problem is expecially difficult in the case of diodes for the formation of helical electron beams used in gyrotrons because such beams must have high transverse momentum as well as low velocity spread and are sensitive to space charge forces. Most gyrotron electron gun designs are based on the use of electron trajectory codes; however, the complexity of the problem is such that a design procedure using only a simulation code can be very tedious and expensive. For these reasons one dimensional approximations to the flow are extremely useful. Such one dimensional flows can be used to synthesize first approximations to the electrode shapes. The purpose of this paper is to show how previous work on this technique for non-relativistic beams can be extended to the relativistic intense electron beam regime.

The analysis is based on four one dimensional planar or conical models for electron flow in diodes. The planar models are relativistic and can be used to obtain electrode shapes for space charge limited flow. The conical models shed light on important geometric effects. Principally, it is shown that the space charge limited current is larger in realistic geometries than in the corresponding planar configuration. A design procedure based on these flow models is illustrated by application to a diode for a 1 GW beam for a 35 GHz gyrotron.

CONTENTS

ONE DIMENSIONAL MODELS FOR RELATIVISTIC ELECTRON BEAM DIODE DESIGN

I. INTRODUCTION

The design of a diode, or electron gun, for a microwave tube is a complicated two dimensional spatial and three dimensional velocity space problem. It involves a calculation of nonlinear particle orbits and self consistent electric and magnetic fields. The design problem is especially difficult in the case of diodes for the formation of helical electron beams used in gyrotrons because such beams must have high transverse momentum as well as low velocity spread and are sensitive to space charge forces. In virtually all diode design work, the basic tool is an electron trajectory code (Herrmannsfeldt 1979) which solves for the electron orbits and the self consistent electric and magnetic fields in an arbitrary two dimensional configuration. Since this problem is so complex and the parameter space so vast, a design procedure using only a flow simulation code can be very tedious and expensive. Also, since the electron trajectory code begins with vacuum fields as a first approximation, it is often difficult to converge on flow solutions with strong space charge effects. For these reasons, one dimensional approximations to the physics are extremely useful. This is particularly true for space charge limited diodes, suitable for intense relativistic electron beams which are of interest for high power gyrotrons.

The basis of this paper, and many other works in this area, is that there are useful one dimensional approximations to the orbit in an infinite medium. Then the infinite medium approximation is relaxed by taking only a spatially limited part of the infinite flow pattern, and focusing electrodes are used to create the fields set up by the remainder of the beam which was excluded (Harker 1960a, 1960b; Dryden 1962; Kirstein, Kino and Waters 1967; Tsimiring 1972, Manuilov and Tsimring 1979; and Fliflet et al. 1982). The shapes of the focusing electrodes are determined by the particle orbit. Along the orbit, both the potential and its normal derivative are known. Laplace's equations must then be solved exterior to this orbit to determine the equipotentials (that is, the shape of the focusing electrodes). However, the solution in the open exterior region is unstable. To determine the solution, a scheme based on conformal mapping is used. The orbit equation is rewritten as an equation valid in the complex plane. Then the potential is calculated by for real r and imaginary z at some fixed value of real z. This involves the solution of a wave equation, which has stable solutions for *Cauchy* boundary conditions on an open surface. Evaluating the solution at the imaginary part of $z=0$ gives the potential as a function of r at the fixed value of the real part of z chosen. Thus, a stable solution is

Manuscript approved December 15, 1985.

built up by taking a two dimensional projection of a solution in three dimensions. The equipotentials are then appropriate places for the location of focusing electrodes.

The only trouble with this method is that once the beam becomes relativistic, and/or self magnetic fields become important, as is the case with intense pulsed beams, there is no one dimensional model which describes the flow. This paper derives a variety of approximate one dimensional models for space charge limited flow in a diode with an applied magnetic field. While no model is exact (the electron flow is inherently two dimensional), they provide important insight and allow for approximate synthesis of the electrodes. The actual electrodes can then be quickly perfected with the Herrmannsfeldt code.

Finally, we note other attempts at one dimensional models. A model similar to one of those in the next section, but with the magnetic field parallel to the cathode plane has been derived by Goldstein (1976). Another approximate model, valid in planar, cylindrical or spherical geometry is the Brillouin model of Creedon (1975). Here the self magnetic fields are assumed so strong that electrons flow on equipotential surfaces, so that the model does not describe the emission from an electrode. Another model (Ott et al. 1977) describes the electrostatic field in two dimensions, but the electron flow in one dimension. Finally, we note an approximate two dimensional analytic model of focused electron flow in diodes (Goldstein et al. 1974).

Section II describes four one dimensional models for electron flow in diodes. The first two are planar, relativistic but either with or without self magnetic fields. The second two are conical, with no self magnetic fields, and either nonrelativistic or superrelativistic. The nonrelativistic, but not the superrelativistic model, is well known and has been used in several applications. The last model can in principle accommodate self magnetic fields, although we have not exploited this feature. We rely mostly on the planar models since they are valid over the full energy range. However there are still important geometric effects, and the conical models shed light on them. Principally it is shown in Section III that the space charge limited current is larger in realistic geometry than in the analogous planar configuration. Section IV reviews the electrode synthesis technique and derives electrodes for a relativistic beam in a planar configuration. Finally, Section V derives a final electrode configuration using the Herrmannsfeldt code. The goal is to achieve a high quality beam for use in a gyrotron oscillator at 35 GHz and with power in the hundred megawatt range. Accordingly, the diode has a magnetic field of 1.8 – 2.0 kG and produces a 600 kV, 2 kA beam with $\alpha \equiv v_\perp / v_\parallel = 0.2$. In the diode region and subsequent drift space, the beam has virtually no variation in α. To achieve the higher values of α, the magnetic field must be compressed to about 25 kG. In doing so, some variation in α across the beam is induced, although the beam quality is more than sufficient for efficient oscillator operation.

II. ONE DIMENSIONAL MODELS

In this section we describe three separate one dimensional models which should be of use in the design of a wide class of diodes. These models are, respectively, a relativistic slab model, a conical nonrelativistic model, and a conical superrelativistic model. No fully relativistic one dimensional conical model was found. We have used the slab relativistic model to explore a large area of parameter space for interesting design candidates. This model is used in the electrode synthesis described in Section IV. The conical models were used to estimate geometric corrections to the slab designs, specifically the current required to obtain space charge limited flow.

A. Slab Relativistic Model

The slab diode is completely described by three constants of motion for every particle, namely energy and the canonical momenta P_y and P_z. Here, the cathode is the plane $x = 0$ and the anode is at $x = L$. The coordinate z corresponds to length along the cathode face and the magnetic field $\mathbf{B}$ is in the x–z plane. [The coordinate y corresponds to the azimuthal angle ϕ in the more conventional cylindrically symmetric diode.] For any particle which leaves the cathode $x = 0$, these invariants of motion are

$$\Delta E = (\gamma - 1)mc^2 + q\,\Phi\,(x), \tag{1}$$

$$P_y = \gamma\, mv_y - \frac{qB_{x0}}{c}(z - z_0) + \frac{q}{c}\tilde{A}_y(x) \tag{2}$$

$$P_z = \gamma\, mv_z + \frac{qB_{x0}}{c}(y - y_0) + \frac{q}{c}\tilde{A}_z(x) \tag{3}$$

where y_0, z_0 give the initial position of the particle. The constant of motion P_y is the canonical momentum associated with y in the gauge with $A_y = \tilde{A}_y(x) + B_{x0}\,x - B_{z0}\,z$, $A_z = \tilde{A}_z(x)$. The third constant of motion P_z is the canonical momentum associated with z in another gauge, with $A_y = \tilde{A}_y(x) + B_{z0}\,x$, $A_z = \tilde{A}_z(x) + B_{z0}\,x$. Because of the gauge change the Poisson bracket between P_y and P_z is not zero. However, this is not important for our applications. In both gauges $\tilde{A}$ and $\tilde{\Phi}$ correspond to self fields and B_{x0}, B_{z0} are the externally applied fields. In Eqs. (2) and (3), $\tilde{A}_y = \tilde{A}_y + B_{z0}\,x$, $\tilde{A}_z = \tilde{A}_z$, i.e., $\tilde{\mathbf{A}}$ represents all the fields but B_{z0}. Constants have been added so that the invariants of the motion are zero on the cathode ($x = 0$) and Φ, $\tilde{A}$, $\tilde{\Phi}$ are also zero there. Because of y,z symmetry only one orbit needs to be considered; without loss of generality it can have $y_0 = z_0 = 0$. From Eqs. (1)-(3) and the definition of γ we find

$$v_x(x, y, z) = \left[\begin{array}{c} \\ \\ \end{array}\right] \tag{4}$$

$$v_y(x,z) = \frac{\Omega_x z}{\gamma(x)} - \frac{q}{mc\gamma(x)} \hat{A}_y(x), \tag{5}$$

$$v_z(x,y) = -\frac{\Omega_x y}{\gamma(x)} - \frac{q}{mc\gamma(x)} \hat{A}_z(x), \tag{6}$$

where $\Omega_x = qB_x/mc$ and $\gamma(x) = 1 - q\Phi/mc^2$, from (1). Since v_x is chosen to be positive in (4), these equations will apply only up to the first turning point in x. This is exactly the condition that no orbits cross.

If a steady source of current j_0 is supplied at the cathode, an equilibrium state will be set up with $j_x = j_0$ (by $\nabla \cdot \mathbf{j} = 0$) with density

$$n = \frac{j_0}{q v_x}.$$

Thus, Poisson's and Ampere's equations give, respectively,

$$\frac{d^2\Phi}{dx^2} = \frac{4\pi j_0}{v_x}, \tag{7}$$

$$\frac{d^2\hat{A}_z}{dx^2} = \frac{4\pi j_0 v_z}{v_x c}, \tag{8}$$

$$\frac{d^2\hat{A}_y}{dx^2} = \frac{4\pi j_0 v_y}{v_x c} \tag{9}$$

$$dy/dx = v_y/v_x, \tag{10}$$

$$dz/dx = v_z/v_x. \tag{11}$$

The equations (7)-(11) can be integrated with the aid of Eqs. (4)-(6) using x as the independent variable as an initial value problem from $x = 0$. The initial conditions imposed are $y = 0$, $z = 0$, $\Phi = 0, \hat{A}_y = \hat{A}_z = 0$, (all by convention), $\frac{d\Phi}{dx} = 0$ (space charge limited flow), $d\hat{A}_z/dx = 0$ ($B_y = 0$, corresponding to $B_\phi = 0$ in the actual diode) and $d\hat{A}_y/dx = B_{z0}$. The current j_0 can be adjusted to provide any positive potential at a given anode-cathode gap spacing, $\Phi(L) = V$. For $B_{z0} = 0$ and in the nonrelativistic limit, these equations give $y = z = A_y = A_z = 0$, and the Langmuir-Child solution $\Phi \sim j_0^{2/3} x^{4/3}$. A typical numerical solution of the equation for nonzero B_z is shown in Fig. 1. Time does not occur explicitly in the equations we integrate. Nevertheless, the best results are obtained by using a uniform time step, i.e., with $dx = v_x dt$. This gives the best resolution of the gyro-motion in the magnetic field and the singular behavior near the cathode, where the solution approximates Langmuir-Child, even with $B_z \neq 0$.

An equilibrium fully symmetric with respect to y and z is obtained if j_0 is a constant. The synthesis discussed in Section IV provides electrode shapes external to the electron beam such that the beam will remain symmetric with respect to y and z if j_0 is uniform in a finite emitting region $0 < z < L_e$ (but $-\infty < y < \infty$, corresponding to $0 < \phi < 2\pi$). However, it is not possible to obtain the correct A_z by such a method, because B_y is proportional to the current I_z within the orbit (see Fig. 1.). For $v_y > 0$ this is zero for the bottom orbit (from the right end of the emitting region) and increases for orbits emitted further to the left, but can never be equal to the value obtained in the pure slab limit for $z > L_e$, because some current is thrown out. Alternatively, we could note that with a finite emitting region, B_y becomes a function of x and z. In order to bracket the exact solution for a planar diode with a finite emitting region, we have integrated the equations [2.1-1] with the full $A_z(x)$ and again with $A_z(x) = 0$. The first model is appropriate when the emitting [illegible] of length L_e is very long or for orbits near the top of the beam before they have traveled a distance Δz equal to L_e. The second model is appropriate for $L_e \to 0$ or for orbits near the bottom of the beam. Results obtained from these models will be discussed in Sec. III. The effect of a finite emitting region on A_z, B_y, and for that matter, the effect of j_y upon B_z for the $L_e \to \infty$ case, is negligible for the designs we study because of a strong applied B_z.

B. Conical Nonrelativistic Model

A scaling that reduces the nonrelativistic conical diode problem to one dimension is well known but we include a brief presentation for completeness. We use spherical coordinates (r, θ, ϕ) to describe a diode with cathode at $\theta = \theta_c$, anode at $\theta = \theta_a$, and ϕ symmetry. The relevant equations for $B_z = B_0 = \text{const.}$ and $B_\phi = 0$ (i.e., ignoring self B_ϕ and j_ϕ) are conservation of energy

$$\frac{1}{2} m v^2 + q\Phi(r, \theta) = 0, \tag{2.1-1}$$

conservation of P_ϕ

$$\left(v_r \frac{\partial}{\partial r} + \frac{v_\theta}{r} \frac{\partial}{\partial \theta} \right) \left(mr \sin\theta\, v_\phi + \frac{qB_0}{2} r^2 \sin^2\theta \right) = 0 \tag{2.1-2}$$

and the r component of the equation of motion

$$(\mathbf{v} \cdot \nabla \mathbf{v})_r = \frac{q}{m} \left(-\frac{\partial \Phi}{\partial r} + \frac{1}{2} v_\phi B_0 \sin\theta \right) \tag{2.1-3}$$

Poisson's equation and $\nabla \cdot \mathbf{j} = 0$ give

$$\frac{\partial^2 \Phi}{\partial r^2} + \frac{2}{r} \frac{\partial \Phi}{\partial r} + \frac{1}{r^2 \sin\theta} \frac{\partial}{\partial \theta} \left(\sin\theta \frac{\partial \Phi}{\partial \theta} \right) = -4\pi nq. \tag{2.1-4}$$

$$\frac{1}{r^2}\frac{\partial}{\partial r}\,(r^2 n v_r) + \frac{1}{r\sin\theta}\,\frac{\partial}{\partial\theta}\,(\sin\theta\; n\; v_\theta) = 0. \tag{16}$$

These equations can be reduced to a one-dimensional form, with θ the independent variable, by assuming the scaling

$$\Phi = r^2\,\Phi_0\,(\theta), \tag{17a}$$

$$v = r\,v_0\,(\theta), \tag{17b}$$

$$n = n_0\,(\theta). \tag{17c}$$

Equations (13), (14) then reduce to

$$\frac{1}{2}\,m\,v_0^2\,(\theta) + q\,\Phi_0\,(\theta) = 0, \tag{18}$$

$$v_{\theta 0}\,dQ/d\,\theta + 2\,v_{r0}\,Q(\theta) = 0, \tag{19}$$

where

$$Q(\theta) = \sin\theta\; v_{\phi 0} + \Omega_0 \sin^2\theta/2 \tag{20}$$

and $\Omega_0 = q\,B_0/mc$. Equation (14) gives

$$v_{\theta 0}\,(\theta)\,\frac{d\,v_{r0}}{d\theta} + v_{r0}^2 - v_{\theta 0}^2 - v_{\phi 0}^2 = \frac{q}{m}\left(-2\Phi_0\,(\theta) + \frac{v_{\phi 0}\,(\theta)\;B_0\sin\theta}{c}\right). \tag{21}$$

From (15) and (16) we obtain

$$\frac{1}{\sin\theta}\,\frac{d}{d\theta}\left(\sin\theta\,\frac{d\Phi_0}{d\theta}\right) + 6\,\Phi_0\,(\theta) = -\,4\pi q\; n_0\,(\theta), \tag{22}$$

$$\frac{1}{\sin\theta}\,\frac{d}{d\theta}\left[\sin\theta\; n_0\,(\theta)\; v_{\theta 0}(\theta)\right] + 3\; n_0(\theta)\; v_{r0}\,(\theta) = 0. \tag{23}$$

We integrate (19), (21), and (22) with respect to θ to obtain $v_{\phi 0}(\theta)$, v_{r0}, and Φ_0, respectively, in addition to finding $r(\theta)$, $\phi(\theta)$ by

$$\frac{d}{d\theta}\,(\ln r) = \frac{v_{r0}}{v_{\theta 0}}, \tag{24}$$

$$\frac{d\phi}{d\,\theta} = \frac{v_{\phi 0}}{\sin\theta\; v_{\theta 0}}. \tag{25}$$

Finally, n_0 and $v_{\theta 0}$ are obtained from (23) and (18)

Note that self magnetic fields cannot be incorporated into these similarity solutions since the dynamical equations (13), (14) require $\mathbf{B} = \mathbf{B}_0(\theta)$, $\mathbf{j} = nq\,\mathbf{v} = r\,\mathbf{j}_0(\theta)$ [i.e., (17b) and (17c)] which cannot satisfy $\nabla \times \mathbf{B} = 4\pi\,\mathbf{j}/c$.

C. Conical Superrelativistic Limit

In the limit of superrelativistic electron energies, $\gamma \gg 1$, Eqs. (12)-(14) are replaced by

$$\gamma\, mc^2 + q\,\Phi = 0, \tag{22}$$

$$\left(v_r \frac{\partial}{\partial r} + \frac{v_\theta}{r}\frac{\partial}{\partial \theta}\right)\left(r \sin\theta\, p_\phi + \frac{q}{c} r\, A_\phi\right) = 0, \tag{23}$$

$$(\mathbf{v}\cdot\nabla\,\mathbf{p})_r = \frac{q}{m}\left(-\frac{\partial\Phi}{\partial r} + v_\theta B_\phi - v_\phi B_\theta\right) \tag{24}$$

where $\mathbf{p} = \gamma\, m\,\mathbf{v}$ and $\gamma = (1 + p^2/m^2c^2)^{1/2}$ becomes $\gamma = |\mathbf{p}|/mc$, i.e., $|\mathbf{v}| = c$. Equations (15)-(17) are unchanged. One dimensional equations in θ are obtained in this limit by the following ansätze:

$$\Phi = r\,\Phi_0(\theta) \tag{25a}$$

$$\mathbf{p} = r\,\mathbf{p}_0(\theta) \tag{25b}$$

$$\mathbf{v} = \mathbf{v}_0(\theta) \tag{25c}$$

$$\gamma = r\,\gamma_0(\theta) \tag{25d}$$

$$\mathbf{B} = \mathbf{B}_0(\theta) \tag{25e}$$

$$\mathbf{A} = r\,\mathbf{A}_0(\theta) \tag{25f}$$

$$n = n_0(\theta)/r. \tag{25g}$$

Note that $n\mathbf{v}$ and $\nabla \times \mathbf{B}$ both scale as $1/r$, so that self fields can be included in these solutions. Equations (26), (27) give

$$\gamma_0(\theta)\, mc^2 + q\,\Phi_0(\theta) = 0, \tag{26}$$

$$p_{\theta 0}\frac{dQ}{d\theta} + 2p_{r0}Q = 0, \tag{27}$$

with

$$Q(\theta) = \sin\theta\, p_{\phi 0} + q\, A_{\phi 0}(\theta)/c \tag{28}$$

Equations (28), (15) and (16) give

$$v_{\theta 0}\frac{dp_{r0}}{d\theta} + v_{r0}\,p_{r0} - v_{\theta 0}p_{\theta 0} - v_{\phi 0}\,p_{\theta 0}$$

$$= q\left\{-\Phi_0 + \frac{v_{\theta 0}\,B_{\phi 0} - v_{\phi 0}\,B_{\theta 0}}{c}\right\} \tag{33}$$

$$\frac{1}{\sin\theta}\frac{d}{d\theta}\left(\sin\theta\,\frac{d\Phi_0}{d\theta}\right) + 2\Phi_0 = -4\pi q n_0, \tag{34}$$

$$\frac{1}{\sin\theta}\frac{d}{d\theta}\left(\sin\theta\,n_0\,V_{\theta 0}\right) + n_0\,v_{r0} = 0. \tag{35}$$

The θ component of Ampere's law gives $B_{\phi 0} = -n_0 q\,v_{\theta 0}$, and the r component

$$\frac{1}{\sin\theta}\frac{\partial}{\partial\theta}\left(\sin\theta\,B_{\phi 0}\right) = n_0\,q\,v_{r0}$$

is consistent by (35). The ϕ component of Ampere's law gives

$$B_{\theta 0} = -2\,A_{\phi 0}, \tag{36a}$$

$$\frac{d}{d\theta}\left[\frac{1}{\sin\theta}\frac{d}{d\theta}\left(\sin\theta\,A_{\phi 0}\right)\right] + 2\,A_{\phi 0} = -n_0\,q\,v_{\phi 0}. \tag{36b}$$

Equations (30)-(36), together with (24) and (25) can be integrated as initial value equations from $\theta = \theta_0$ as in the planar and nonrelativistic conical diode cases. When the self magnetic fields are negligible, $B_{\phi 0} = 0$, $B_{\theta 0} = -2\,A_{\phi 0} = -B_0 \sin\theta$ and (36b) is not used.

III. APPLICATIONS OF ONE DIMENSIONAL MODELS

In this section we describe how the one dimensional models of Sec. II are used in diode design. The slab relativistic model has been used primarily to scan the parameter space for reasonable design candidates. Electrode synthesis has been applied to the promising designs, with further electrode shaping required both for final tuning of the design and for other practical considerations. This model has been used to shed light on certain aspects of the design, for example, the dependence of the results on the self B_ϕ. The conical models have been used to clarify the geometric effects, specifically the variation of the space charge limited current obtained by the Hermansfeldt code from the value predicted by the slab model. Let us assume that we want to produce a beam with $\alpha \equiv |p_\perp/p_\parallel| \approx 1$ in an interaction region of radius $r_f = 1.4$cm, with a field $B_{zf} = 24$ kg. Assuming that the beam is adiabatic in the drift region between the diode and the interaction region, i.e.,

$$\frac{B_i}{B_f} = \frac{1 + 1/\alpha_f^2}{1 + 1/\alpha_i^2} \tag{37}$$

and

$$r_i = r_f \, (B_f/B_i)^{1/2}, \tag{38}$$

and taking $\alpha_i = 0.2$, we obtain $B_i = 1.85$kg, $r_i = 5.05$ cm.

We have used the slab relativistic model to compute α at the anode as a function of the angle χ_0 between the normal to the cathode and the externally imposed magnetic field, i.e., $\chi_0 = \tan^{-1}(B_{z0}/B_{x0})$. The gap voltage was $\Phi = 600$ kV, and the current density j_0 was 70 A/cm^2. The results, with and without self $B_y(x)$, are shown in Fig. 3. Without B_y, $\chi_0 = 30°$ gives $\alpha_i = 0.2$, whereas with B_y, $\chi_0 = 40°$ is correct. This indicates that self B_y plays an important role in determining α, although it has little influence on the gap spacing d. Since B_y (or B_ϕ) is zero for the bottom orbit, and since B_y (B_ϕ) can be near its limiting one dimensional value for orbits near the top, this indicates that electrode synthesis may not by itself produce a uniform α across the beam. We will return to this issue in Sec. V. We also show, in Fig. 4, the dependence of α and d upon j_0, for $\chi_0 = 40°$, $\Phi = 600$ kV, including self $B_y(x)$. It is clear that both of these quantities depend critically upon j_0.

As we shall discuss further, the Hermannsfeldt code in this parameter range shows space charge limited flow at 20-50% higher current than that indicated by the slab model. In order to understand this discrepancy and have more confidence in our results, we have investigated this effect with the nonrelativistic and superrelativistic conical models. We use these models in the following manner: we fix the cathode angle θ_0 (see Fig. 2), a potential Φ, a gap spacing d, a field B_{z0}, and a radius R where a ray is to be emitted. We adjust j_0 until the potential equals Φ when the gap spacing is d. Then we vary R. The results for different R values are not obtainable from the scalings (17) or (29) because we do not allow Φ and d to scale appropriately with R [$\Phi \sim R^2, d \sim R$ from (17) or $\Phi \sim R$, $d \sim R$ from (29)]. For a case with $\Phi = 1.07$ MV, $B_{z0} = 2.4$kg, $d = 3$cm, $\theta_0 = 158°$, we obtain the results shown in Fig. 5. For both the nonrelativistic and superrelativistic models, the results fit curves of the form $j_0 = j_0(\infty) + A/R$, and the limiting value $j_0(\infty)$ agrees with corresponding slab nonrelativistic or slab superrelativistic models. For the cases considered, j_0 for $R = 5$ cm is 20 to 50% higher than for the slab model, in agreement with the results obtained using the Hermannsfeldt code.

IV. SYNTHESIS TECHNIQUE FOR DETERMINING ELECTRODE SHAPES

The electrode synthesis technique is a method of calculating electrode shapes which provide laminar flow for a beam with self electric fields. The method was initially formulated by Harker for planar and axially symmetric cases of space charge limited nonrelativistic flow. The method was extended to temperature-limited MIG type guns by Manuilov and Tsimring. The general approach involves finding a set of ordinary differential equations to represent the beam flow. These equations are used to obtain the boundary conditions for integrating Laplace's equations in the region outside the beam. A difficulty

in the direct inplementation of this procedure is that the present problem involves Cauchy boundary conditions on an open surface and the solutions of Laplace's equation are unstable for these conditions. An elegant method has been developed by Harker which reformulates the mathematical problem in a way which yields stable numerical solutions. This section outlines the synthesis technique for planar geometry and discusses an application for the case of planar relativistic flow.

The synthesis problem consists of finding the electrostatic potential distribution in a region external to a finite laminar flow beam. The potential satisfies Laplace's equation outside the beam or equivalently, the electrostatic field satisfies the Maxwell divergence and curl equations

$$\frac{\partial E_x}{\partial x} + \frac{\partial E_z}{\partial z} = 0 \tag{39}$$

$$\frac{\partial E_x}{\partial z} - \frac{\partial E_z}{\partial x} = 0 \tag{40}$$

with the boundary conditions

$$E_z = E_{ze}, E_x = E_{xe} \tag{41}$$

on the outermost trajectory of the beam.

Equations (39) and (40) form a system of elliptic partial differential equations whose solutions are unstable for the present case of an open surface and Cauchy boundary conditions. However, a stable solution can be obtained by the following approach due to Harker.

First, the beam edge trajectory ($x_e = x_e(t)$, $z_e = z_e(t)$), is converted into the straight line $u = 0$ of the (t,u) plane by means of the conformal transformation

$$z + ix = z_e(t + iu) + ix_e(t + iu). \tag{42}$$

This can be done because the equations for the beam trajectory can be expressed in the complex plane by analytic continuation. Since coordinates related by a conformal transformation satisfy the Cauchy-Riemann conditions,

$$\frac{\partial x}{\partial u} = \frac{\partial z}{\partial t} \tag{43}$$

$$\frac{\partial z}{\partial u} = -\frac{\partial x}{\partial t}. \tag{44}$$

Equations (39) and (40) can be expressed in the form

$$\frac{\partial E_x}{\partial u} = -\frac{\partial E_z}{\partial t} \tag{45}$$

$$\frac{\partial E_z}{\partial u} = \frac{\partial E_x}{\partial t}. \tag{46}$$

These equations, together with

$$\frac{\partial \Phi}{\partial u} = -E_x \frac{\partial z}{\partial t} + E_z \frac{\partial x}{\partial t} \tag{47}$$

enable calculation of the potential Φ in the transformed plane (t,u).

The second step is the transformation of the elliptic system, Eqs. (45) and (46) in the (t,μ) plane, by means of the analytic continuation

$$t \rightarrow p + iq \tag{48}$$

For fixed p this leads to the hyperbolic system in the (q,u) plane:

$$\frac{\partial E_x}{\partial u} = i\frac{\partial E_z}{\partial q} \tag{49}$$

$$\frac{\partial E_z}{\partial u} = -\frac{i\,\partial E_x}{\partial q} \tag{50}$$

$$\frac{\partial x}{\partial u} = -\frac{i\,\partial z}{\partial q} \tag{51}$$

$$\frac{\partial z}{\partial u} = \frac{i\partial x}{\partial q} \tag{52}$$

Equations (49) and (52) have a stable solution for the present boundary conditions.

The procedure for obtaining the equipotentials is illustrated in Fig. 6. It involves solving the system (49) and (52) in triangular regions such as ABC in Fig. 6. To obtain the solution for this region it is sufficient to specify Cauchy boundary conditions on the line AB. These conditions are the analytic continuation of Eq. (41) and are formed by integrating the flow equations along the real axis from $t = 0$ to $t = P_D$ and then along the line AB by means of the substitution

$$\frac{d}{dt} \rightarrow i\frac{d}{dq}. \tag{53}$$

Solving Eqs. (49)-(52) in the region ABC by a finite difference method allows the potential to be obtained on the line CD, the only region of physical significance. By translating the triangle ABC to other values of p, the potential distribution over the entire single valued region of the plane $(p,u) = (t,u)$ can be found. Applying the transformation (42) yields the equipotential surfaces as a function of x and z.

Electrodes shapes calculated by the synthesis technique are shown in Fig. 7 for the planar relativistic flow model discussed in section II A. The synthesis calculation was based on a current density of 70 A/cm^2, an angle of 40° between the cathode normal and the external magnetic field, and an external magnetic field by 1.85 kG. The anode-cathode gap voltage is 600 kV. Upper beam edge trajectories are shown with and without the approximation self magnetic field effect included. As shown the effect is quite small for the present parameters and there is negligible effect on the calculated electrodes.

V. FINAL DIODE DESIGN

The final design for the diode, in several configurations, was achieved by means of an electron trajectory (Hermannsfeldt) code. The electrodes found by synthesis generally provide a beam in which α varies by $\pm$ 50% from top to bottom. This variation, which is not present in the slab model, is due to geometric effects. One of these effects is the fact that the bottom orbit has $B_\phi = 0$, whereas the top orbit has a value of B_ϕ which can be nearly equal to the one-dimensional value (for fat beams). This effect has been studied in Sec. III and found to provide just such a variation in α.

Our first design is for a 600 kV, 2 kA gun which can use a minimal amount of focusing, depending upon intercepting the outer two thirds of the beam at the anode. This extra charge (and current) takes the place of some of the focusing. A successful design of this type is shown in Fig. 8. The cathode face is at 40°, which we found in Sec. III gives $\alpha = 0.2$ with $B_{z0} = 1.85$ kg. The current density $j_0 = 70$A/cm^2 in the slab model gives, for a cathode surface of radius 5 cm and emitting length 2.1 cm, 4.6 kA. Because of geometric effects as discussed in Sec. III, we used 6.0 kA, corresponding to a perveance $k = 13$ micropervs. This is near the space charge limit; for $k \gtrsim 15$, the results begin to show serious signs of lack of convergence usually associated with approaching the space charge limit at some point on the cathode face. The results show a very flat $\alpha \approx 0.2$, $\pm 10\%$ and very little evidence of orbit crossing. It is possible to reshape the electrodes to have less focussing in order to decrease the electric fields on the parts of the cathode where we wish to inhibit emission. In that case α would not be as flat across the whole 6 kA beam, but that is of no consequence. However, it appears that the electric fields in the design in Fig. 6 are below 300 kV/cm, and the surfaces of anodized aluminum on the focusing electrodes should inhibit emission for at least 50 ns.

In Fig. 9 we show a design with an aperture in the anode allowing roughly the middle third of the beam, and a short drift region bounded by anode surfaces. There is very little orbit crossing still, and α is quite flat in the central third of the beam. (For rays intercepted by the anode, the value shown for α is the value at interception.) However, α is considerably higher now, in the range $0.36 < \alpha < 0.41$. This is apparently due to a combination of effects, including the space charge of the beam and the finite Larmor radius of the orbits.

An alternate design for a 600 kV, 2 kA diode is shown in Fig. 10. Here, uniformity of the beam is achieved by focusing electrodes alone; all of the beam is allowed to pass through the aperture in the anode. The electrode shapes are nearly identical to those of the design in Figs. 8 and 9, except that the emitting region is one third the length, or 7mm; the perveance is, correspondingly, $k = 4.3\mu$ microperus and the magnetic field is a nearly uniform 1.85 kg. Again, the electrode shapes are somewhat different from those obtained by synthesis, for geometric reasons, and the maximum electric field is of order 300 kV/cm. Figure 10 shows essentially no orbit crossing in the diode region and a very uniform $\alpha = 0.19 \pm 5\%$ across the beam at the anode and at the end of the drift region. A combination of coils produce a quite uniform 2.2 kg magnetic field in the diode region that increases to 20 kg at the far end of the compression region. The average value of α at the far end of the compression region agrees well with the adiabatic value $\alpha_f = 1.2$ based on $\alpha_i = 0.22$, $B_i = 2.2$ kg at the beginning of the compression region and $B_f = 28$kg at the end. However, there is much more variation in α across the beam than adiabatic theory predicts; from (37) one can show

$$\frac{d\ln \alpha_f}{d\ln \alpha_i} = \frac{2}{1+\alpha_i^2}, \tag{39}$$

which shows that the relative variation in α_f should only be twice the relative variation in α_i for $\alpha_i << 1$. This is a common effect in this type of simulation and is apparently due to space charge effects that become more pronounced as the beam slows up. The results shown in Fig. 10 a,c,d,e are with 25 rays; results with 15 rays as shown in Fig. 10b give very similar results, including the variation of α across the beam.

Tests have been made to determine the sensitivity of the diode performance to variations in B_z and the potential. For these tests, a 600 kV, 2 kA diode with $B_z = 1.85$ kg was used. These tests are important in order to be able to tune an actual device. In addition, it is important to know whether variation of the voltage during the pulse will have deleterious effects. The nominal diode design here has $\alpha = 0.25$ across the beam. Dropping the potential to 450 kV causes the beam to enter the aperture in the anode less than a centimeter below the point where a 600 kV beam enters, so that it appears that a pulse with 450 kV $< \Phi <$ 600 kV will produce a beam that can still fit through the anode aperture. Furthermore, α is nearly unchanged. These results are not sensitive to the perveance. For B_z ten percent below the nominal value, i.e., 1.67 kg, the beam begins to scrape the top of the drift cavity, and α is larger, in the range $0.32 < \alpha < 0.38$. For B_z twenty percent above, i.e., $B_z = 2.22$ kg has $\alpha \approx .20$. Thus it appears that α scales as $1/B_z$, so that varying B_z may be an effective way to obtain a desired α in this type of diode.

An important consideration for realizing the design based on focusing electrodes involves the control of emitting regions under high voltage conditions. If the electric field is too high, everything will

ultimately emit, including the focusing electrodes. The key is to keep the field sufficiently low and the emissivity of the emitter sufficiently high. For instance, it has been determined (Kirkpatrick et al., 1984) that with focusing electrodes of anodized aluminium and emitting surfaces of reactor graphite, currents in the kiloampere range could be generated for 30 nsec without emission, and that the focusing electrodes do not emit for fields as high as 600 kV/cm.

ACKNOWLEDGMENT

This work was supported by the Office of Naval Research, by the Department of Energy through a contract with the Lawrence Livermore Laboratory, and by the Defense Nuclear Agency.

REFERENCES

Creedon J.M. 1975, Relativistic Brillouin Flow in the High *v/gamma* Diode *J. Appl. Phys* **46** 2946.

Dryden, V.W. 1962, Exact solutions for space-charge flow in spherical coordinates with application to magnetron injection guns. *J. Appl. Phys.*, **33**, 3118-3124.

Fliflet, A.W., A.J. Dudas, M.E. Read and J.M. Baird 1982, Use of Electrode Synthesis Technique to Design MIG-Type Guns for High Power Gyrotrons. Int J. Electronics, **53**, 743.

Goldstein, S.A., R.C. Davidson, J.G. Siambis and R. Lee 1974, Focused-Flow Model of Relativistic Diodes. Phys Rev Lett. **33**, 1471.

Goldstein, S.A. 1976, Magnetic Field Effects on the Emission Law of Electron Current from Cathodes. J. Appl Phys., **47**, 894.

Harker, K.J. 1960a, Determination of electrode shapes for axially symmetric electron guns. *J. Appl. Phys.*, **31**, 2165-2170; 1960b, Electrode design for analytical design of axially symmetrical ion guns. Internal Memorandum, Microwave Laboratory, Stanford University, Report No. 1013, NASA CR-54052.

Herrmannsfeldt, W.B., 1979, Electron trajectory program. SLAC-Report-226, Stanford Linear Accelerator Center, Stanford, California.

Kirkpatrick, D.A., R.E. Shefer and G. Bekefi, 1984, High Brightness Electrostatically Focused Emission Electron Gun for Free Electron Laser Applications. MIT Plasma Fusion Center preprint PFC/JA-84-40.

Kirstein, P.T., G.S. Kino, W.E. Waters 1967, *Space-Charge Flow*, McGraw-Hill, New York.

Manuilov, V.N., and Tsimring, Sh.E., 1979, Synthesis of Axially Symmetrical Systems for Shaping Helical Electron Beams. Radio Engng. Electron Phys. **23**, 111.

Ott, E., T.M. Antonsen, Jr., R.V. Lovelace 1977 Theory of Foil-less Diode Generation of Intense Relativistic Electron Beams. Phys. Fluids, **20**, 1180.

Tsimring, Sh.E., 1972, Synthesis of Systems for the Formation of Helical Electron Beams. Radio Phys. Quant. Electron., **20**, 1550.

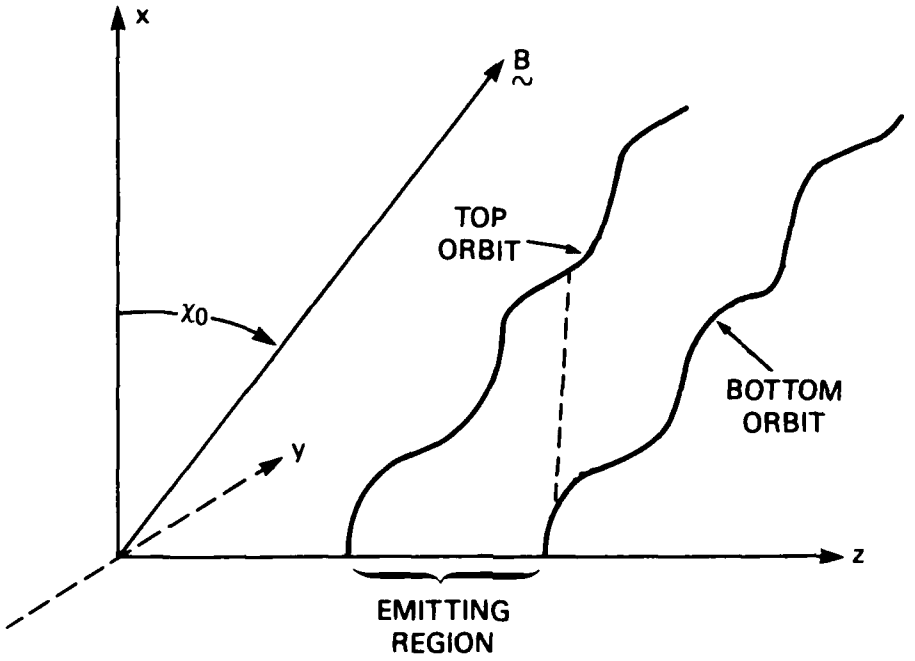

Fig. 1 — Geometry for the slab relativistic diode model. For the bottom orbit, B_y is zero. For the top orbit, B_y is the value obtained by the slab model for electrons to the left of the dashed line. To the right, B_y is less than the slab model value.

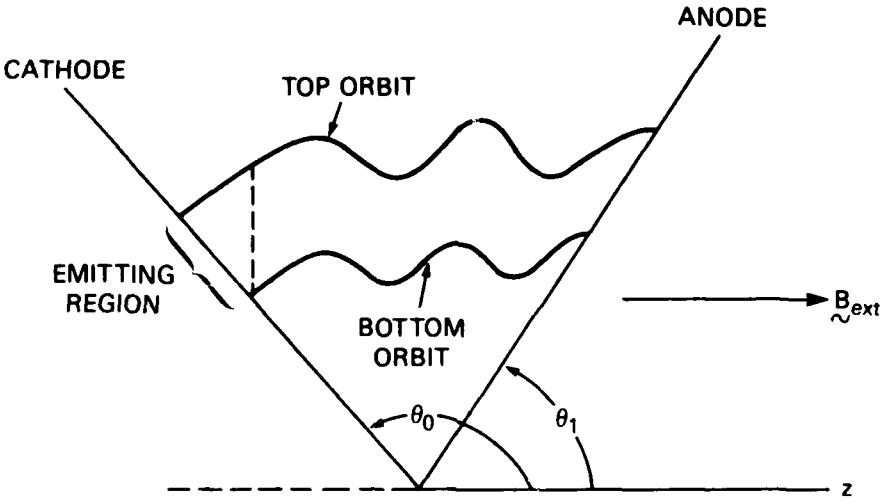

Fig. 2 — Geometry of conical diode. For a finite emitting region, the same comments hold for self B_ϕ. The angle χ_0 of Fig. 1 corresponds to $\theta_0 - \pi/2$.

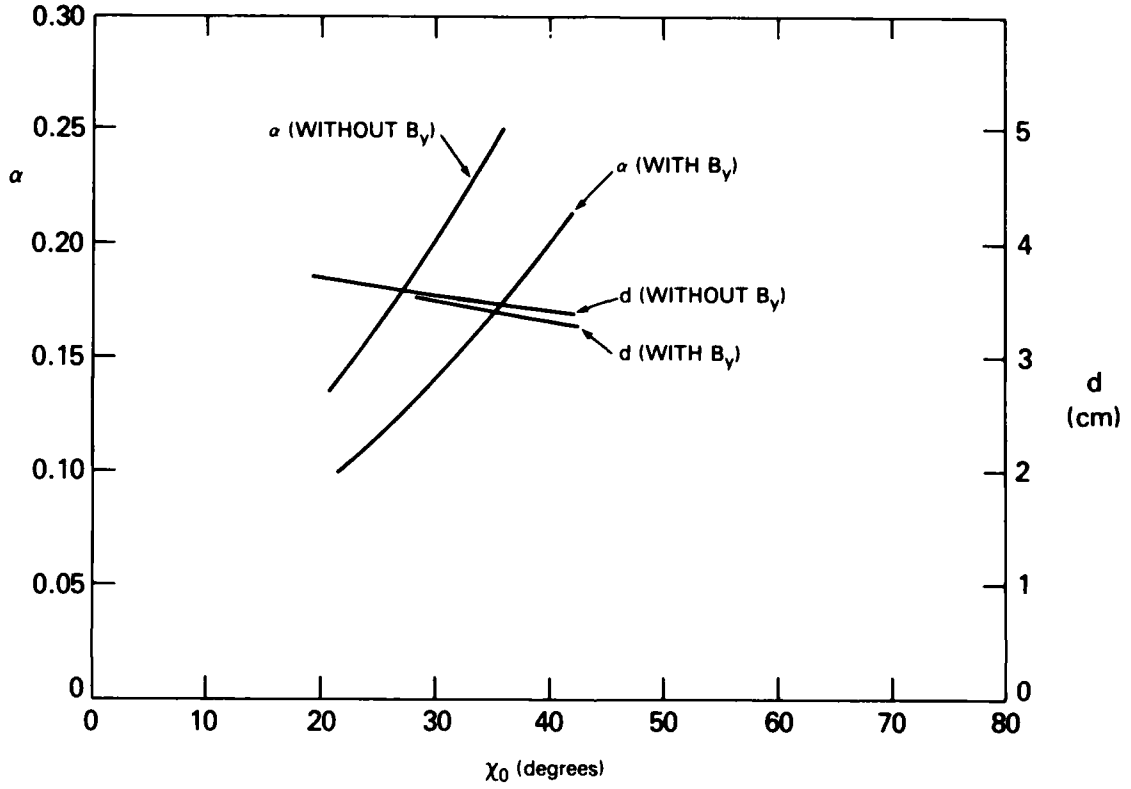

Fig. 3 — Dependence of $\alpha = |p_\perp/p_\parallel|$ and the gap spacing d upon χ_0 for the slab relativistic model

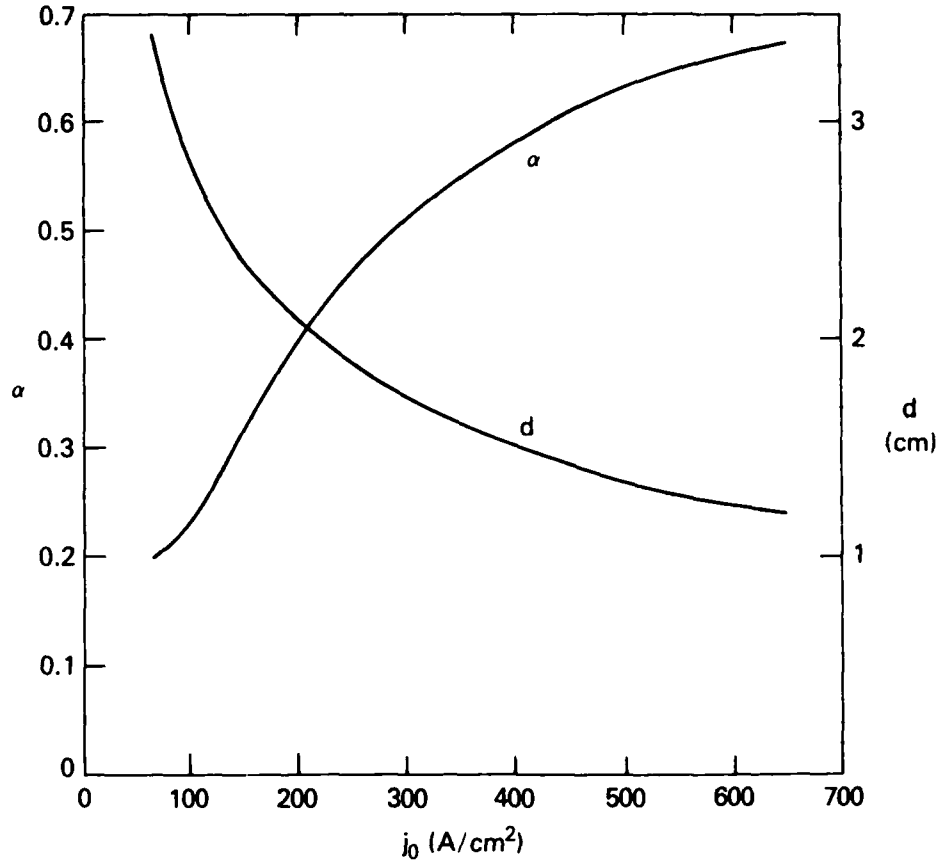

Fig. 4 — Dependence of α and d upon j_0 for the slab model

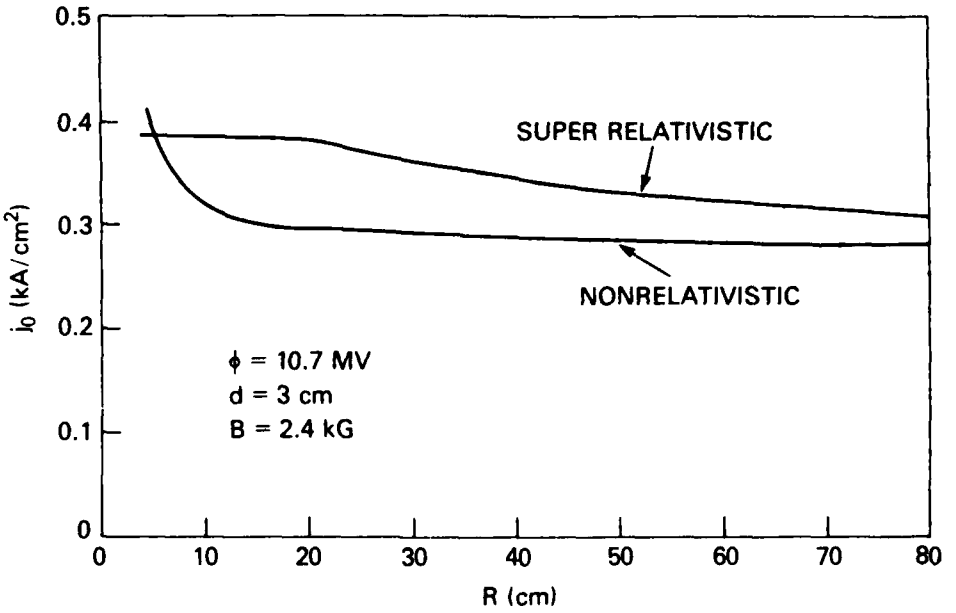

Fig. 5 — Current density j_0 as a function of R for two conical models

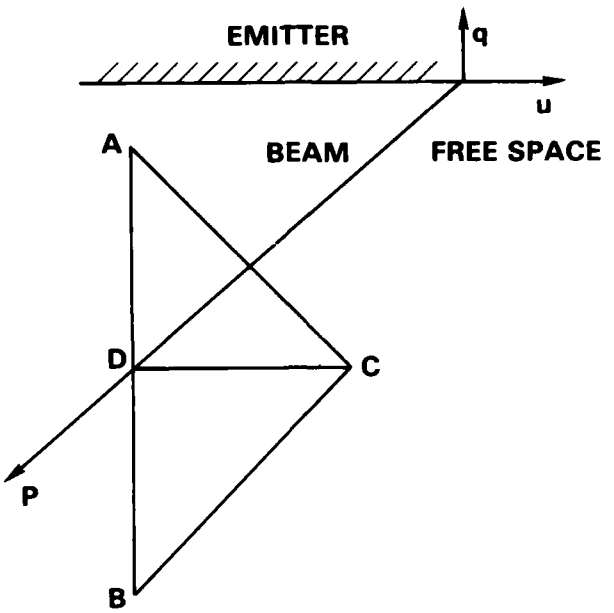

Fig. 6 — Schematic of the solution of Laplace's equation in the complex plane

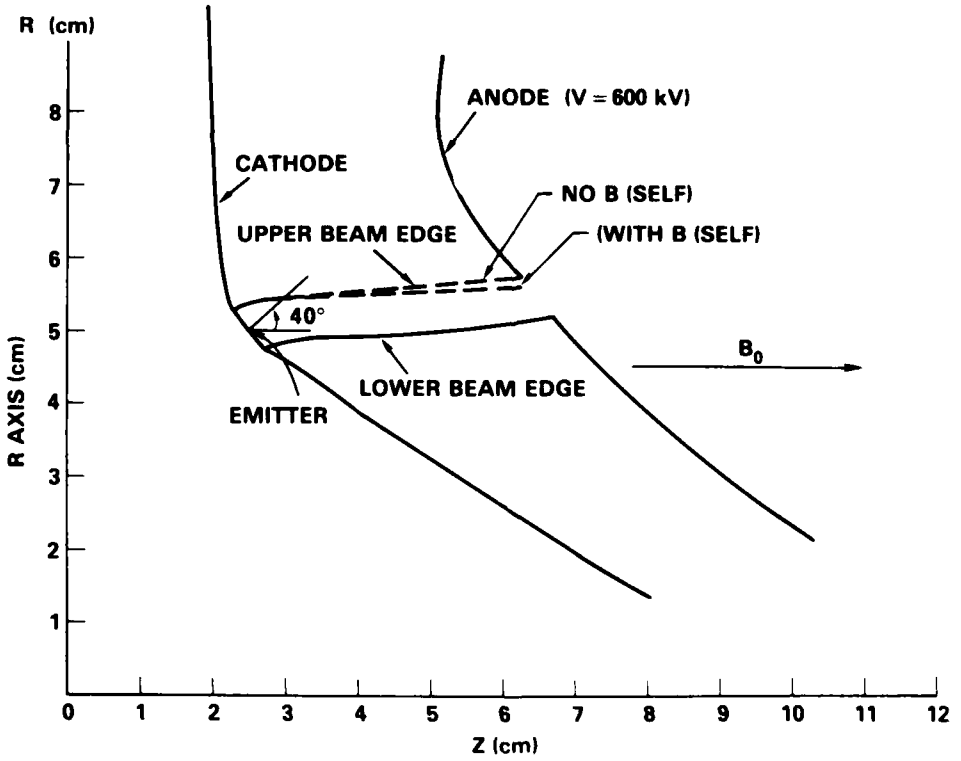

Fig. 7 — Electrode shapes calculated by synthesis technique

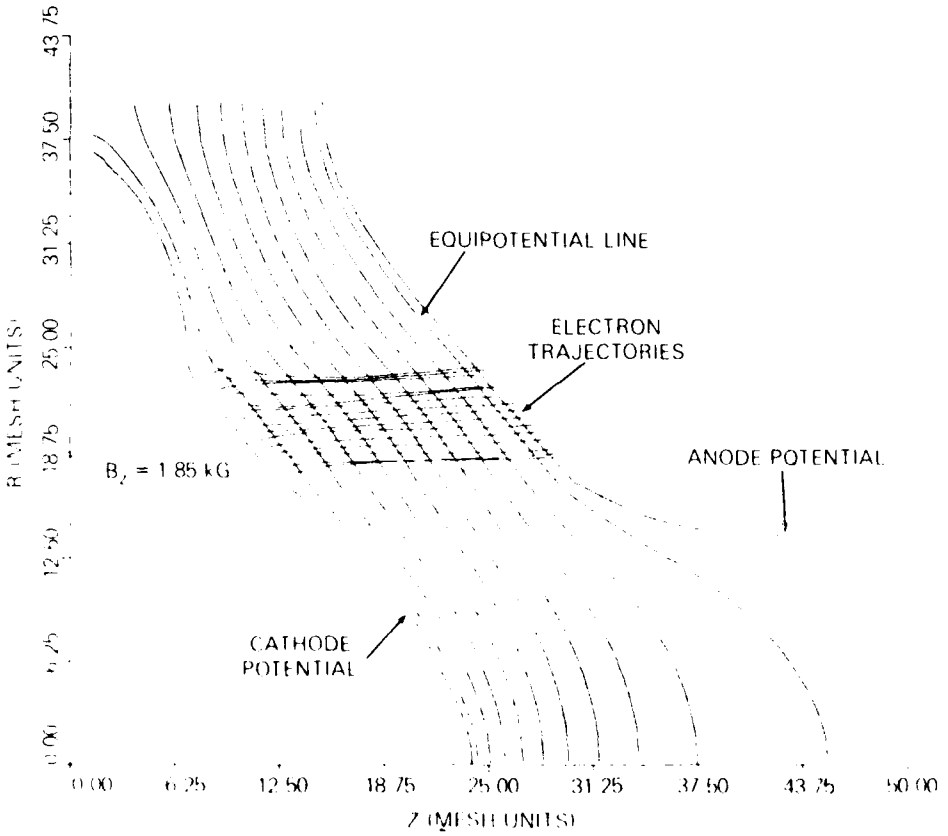

(a)

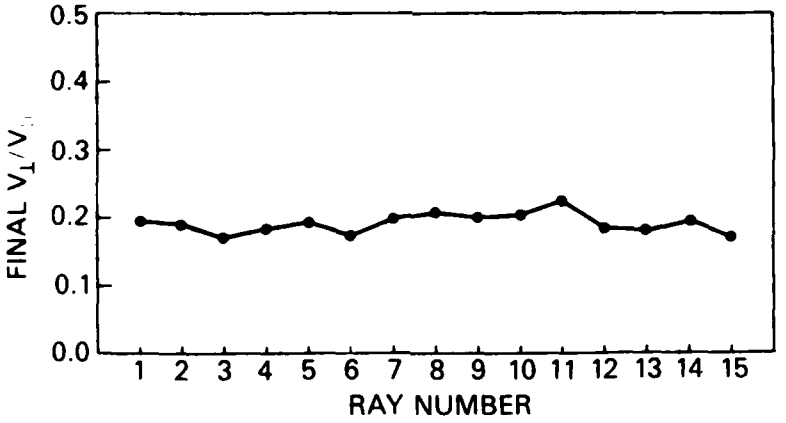

(b)

Fig. 8 — A 600 kV, 2 kA diode design with the outer two thirds of a 6 kA beam to be intercepted by the anode. In (a) are equipotentials and actual trajectories integrated by the code; in (b) is shown α vs ray number, from the bottom of the beam to the top, for the electrons when they hit the anode.

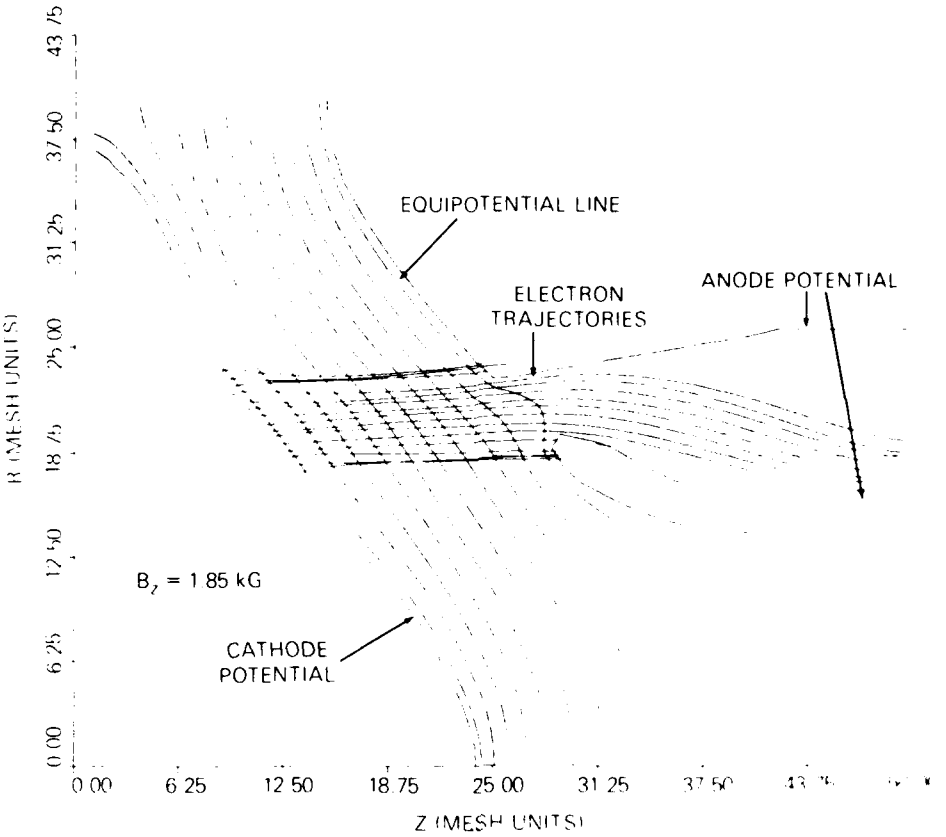

(a)

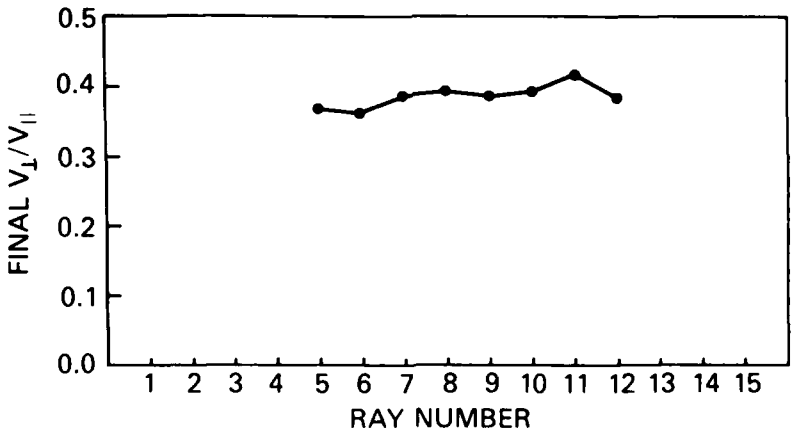

(b)

Fig. 9 — Same diode as in Fig. 8 but with an aperture in the anode and a drift region; (a) equipotentials and trajectories, and (b) α vs ray number at right of drift region.

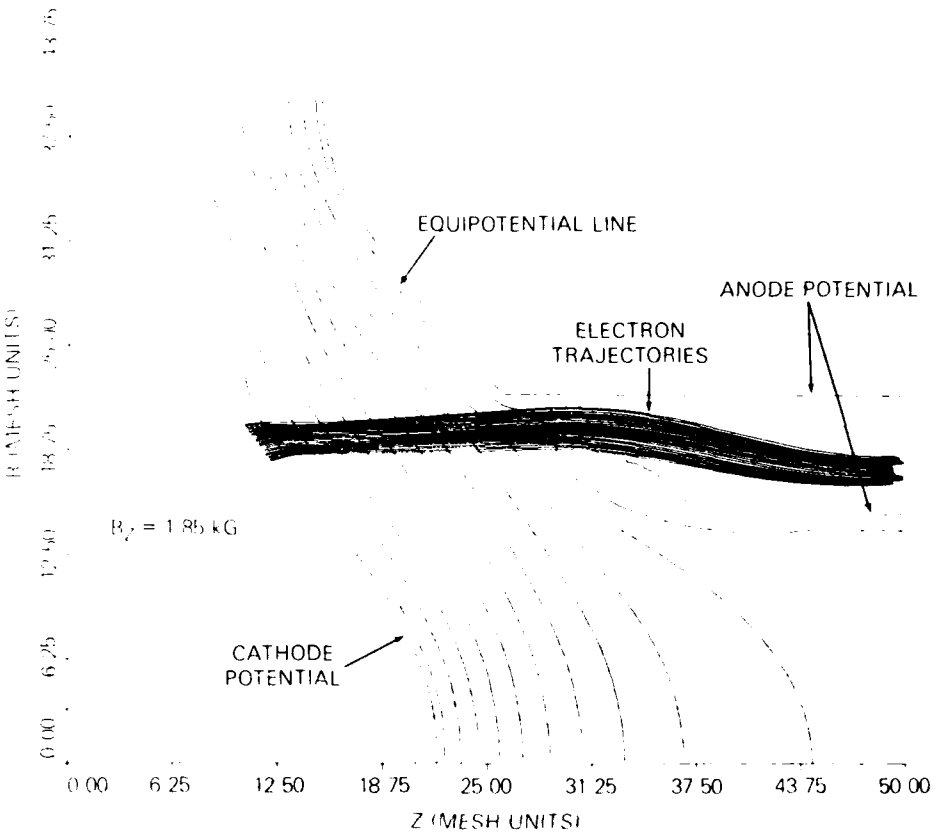

(a)

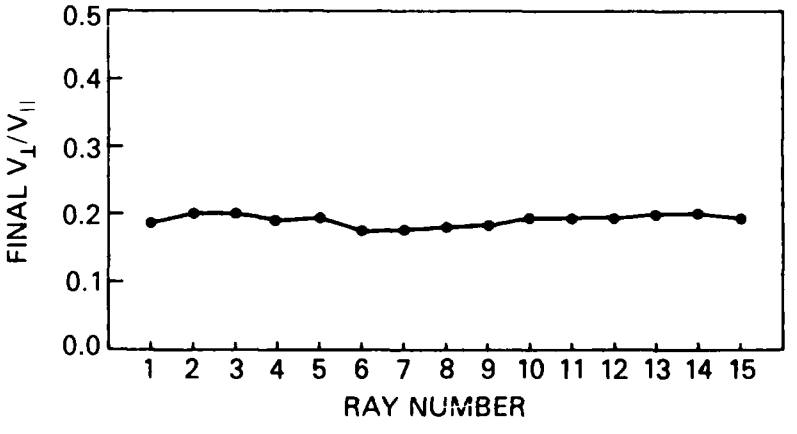

(b)

Fig. 10 — (a) Diode design with 600 kV, 2 kA, where the beam uniformity is provided by focusing electrodes alone, i.e. no interception of beam; (b) α at the aperture in the anode; (c) α at the end of the drift region; (d) orbits in the compression region, (e) α at the end of the compression region

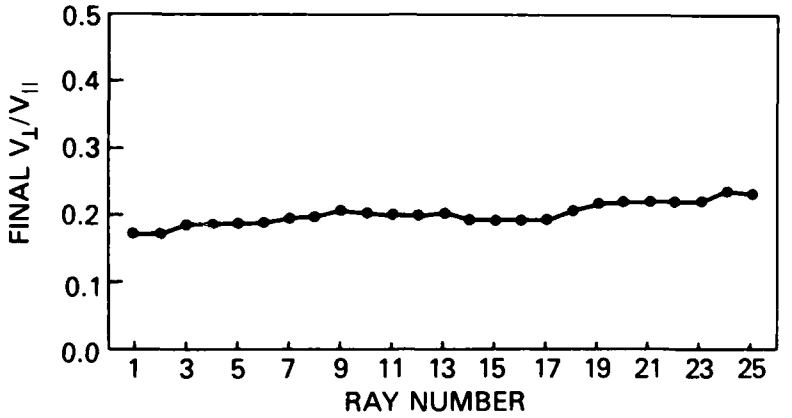

(c)

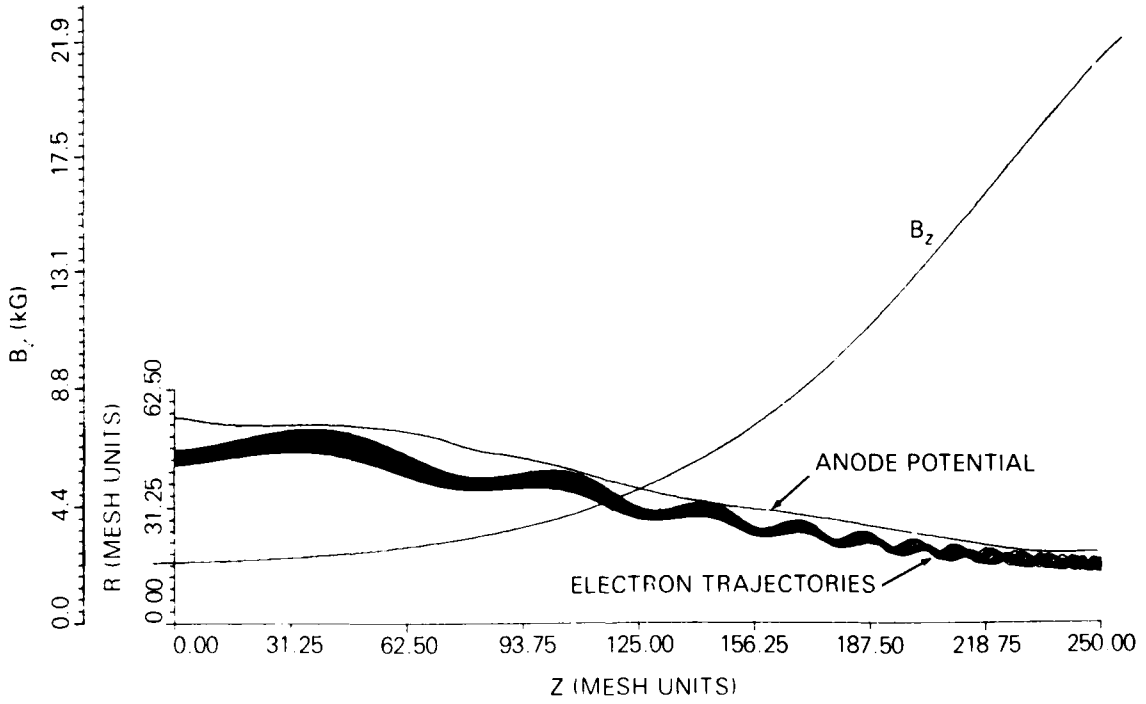

(d)

Fig. 10 (Continued) — (a) Diode design with 600 kV, 2 kA, where the beam uniformity is provided by focusing electrodes alone, i.e. no interception of beam; (b) α at the aperture in the anode; (c) α at the end of the drift region; (d) orbits in the compression region, (e) α at the end of the compression region

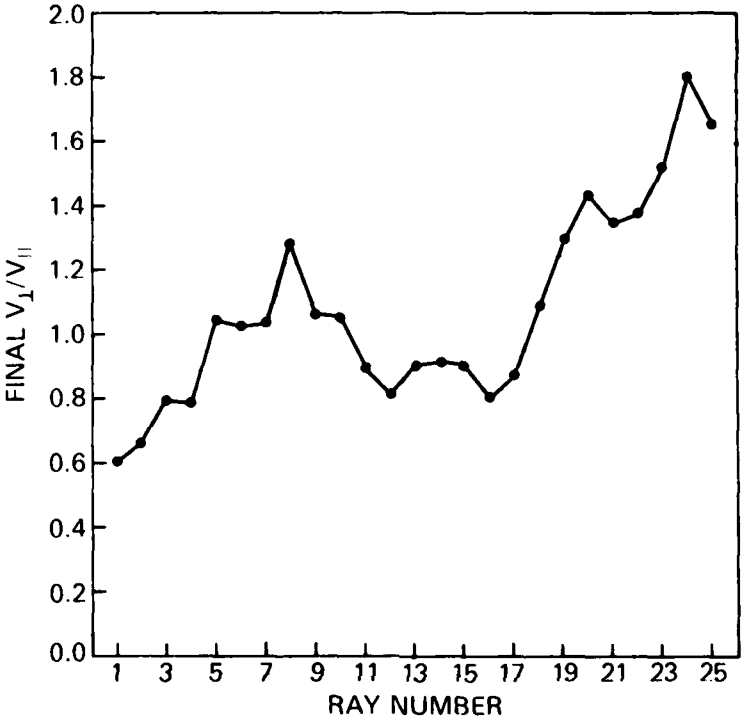

(e)

Fig. 10 (Continued) — (a) Diode design with 600 kV, 2 kA, where the beam uniformity is provided by focusing electrodes alone, i.e. no interception of beam; (b) α at the aperture in the anode; (c) α at the end of the drift region; (d) orbits in the compression region, (e) α at the end of the compression region

END

FILMED

5-86

DTIC